Structure of the Complex of Cdc42Hs with a Peptide Derived from P-21 Activated Kinase[†,⊥]

Dawit Gizachew,[‡] Wei Guo,[‡] Kamaldeep K. Chohan,[§] Michael J. Sutcliffe,[§] and Robert E. Oswald*[,‡]

Department of Molecular Medicine, Cornell University, Ithaca, New York 14853, and Department of Chemistry, University of Leicester, Leicester LE1 7RH, U.K.

Received November 16, 1999

ABSTRACT: Cdc42Hs is a member of the Ras superfamily of GTPases and initiates a cascade that begins with the activation of several kinases, including p21-activated kinase (PAK). We have previously used a 46 amino acid fragment of PAK (PBD46) to define the binding surface on Cdc42Hs [Guo et al. (1998) *Biochemistry 37*, 14030−14037]. Here we describe the three-dimensional solution structure of the Cdc42Hs·GMPPCP−PBD46 complex. Heteronuclear NMR methods were used to assign resonances in the complex, and approximately 2400 distance and dihedral restraints were used to calculate a set of 20 structures using a combination of distance geometry, simulated annealing, and chemical shift and Ramachandran refinement. The overall structure of Cdc42Hs in the complex differs from the uncomplexed structure in two major aspects: **(**1**)** the first α helix is reoriented to accommodate the binding of the peptide and **(**2**)** the regions corresponding to switch I and switch II are less disordered. As suggested by our previous work (Guo et al., 1998) and similar to the complex between Cdc42Hs and fACK [Mott et al. (1999) *Nature 399*, 384−388], PBD46 forms an intermolecular β-sheet with β2 of Cdc42Hs and contacts both switch I and switch II. The extensive binding surface between PBD46 and Cdc42Hs can account for both the high affinity of the complex and the inhibition by PBD46 of GTP hydrolysis.

The rho subfamily of ras-like GTPases,[1] such as Cdc42Hs and Rac, play important roles in the regulation of cell proliferation, differentiation, and cytoskeleton organization (*1*) by binding to different effectors, which initiate a cascade of protein−protein interactions. Activation of Cdc42Hs and Rac initiates a cascade of kinase interactions from the plasma membrane to the nucleus which leads to the activation of two nuclear stress-responsive MAP kinases, JNK1, and p38 (*2*−*5*) and cytoskeletal reorganization (*6*−*8*). A variety of effectors have been identified and include the p85 subunit of the PI3 kinase (*9*), the Wiscott-Aldrich syndrome protein [WASP (*10*), the ACK tyrosine kinase (*11*, *12*), and p21 activated serine/threonine kinase [PAK (*13*, *14*)]. In several cases (e.g., WASP, ACK, PAK), these effectors have a common binding region which is known as CRIB (Cdc42Hs-rac interactive binding) domain (*15*).

We have previously determined the structure of the GDP-bound form of Cdc42Hs (*16*) and have mapped the binding surface on Cdc42Hs for a 46 amino acid peptide derived from PAK [PBD46 (*17*)] using heteronuclear NMR spectroscopy. These results suggested that PBD46 interacts with a β strand (β2) on Cdc42Hs reminiscent of the interaction between Rap1a and Raf-1 (*18*). In addition, however, PBD46 was found to interact with portions of α1, α5, switch I, and switch II. Both switch I and switch II were found to be relatively disordered in the GDP-bound form, with some resonances not observable due to unfavorable dynamics (*16*). However, some resonances (particularly in switch I) which were not detectable in the GDP-bound form could be observed when the protein was bound to PBD46, suggesting that the binding of the peptide modified the dynamic properties of Cdc42Hs (*17*). This was confirmed in a detailed study of the backbone dynamics of Cdc42Hs in the GDP-bound, GMPPCP-bound, and GMPPCP/PBD46-bound forms (*19*). Binding of PBD46 significantly decreased the flexibility of particularly switch I and switch II. The NMR structures of the Q61L mutant of Cdc42Hs complexed to peptides derived from WASP [WASP-GBD (*20*)] and ACK [fACK (*21*)] were reported recently. We present here the three-dimensional structure of the Cdc42Hs·GMPPCP−PBD46 complex. The overall structure of the complex is similar to that of Cdc42Hs·GMPPNP-fACK (*21*); however, some notable differences are present. The flexibility of the binding

[†] This work was supported by a grant from the American Cancer Society and the National Institutes of Health (R01 GM56233) to R.E.O. K.K.C. is a BBSRC Research Committee Special Student.

[⊥] The coordinates of the final 20 structures have been deposited in the Brookhaven Protein Data Bank as entry 1EES.

* To whom correspondence should be addressed. Phone: (607) 253-3877. Fax: (607) 253-3659. E-mail: reo1@cornell.edu.

[‡] Department of Molecular Medicine.

[§] Department of Chemistry.

[1] Abbreviations: fACK, residues 504−545 of ACK tyrosine kinase; GDP, guanosine-5′-diphosphate; GTP, guanosine-5′-triphosphate; GMPPCP, β,γ-methylene derivative of GTP; GMPPNP, β,γ-imino derivative of GTP; PBD46, 44 amino acid portion of the Cdc42Hs binding domain on PAK (mPAK-3; residues 65−108) plus two residues (GS) remaining from cleavage by thrombin; PAK, p21-activated kinase; GEF, guanine nucleotide exchange factor; GDI, GDP dissociation inhibitor; GAP, GTPase activating protein; switch I, residues 31−40 on Cdc42Hs; switch II, residues 57−74 on Cdc42Hs; insert region, residues 118−134 on Cdc42Hs; HSQC, heteronuclear single quantum correlation; NMR, nuclear magnetic resonance; NOE, nuclear Overhauser effect; NOESY, nuclear Overhauser effect spectroscopy; P-loop, residues 10−17 of Cdc42Hs; WASP, Wiskott-Aldrich syndrome protein; WASP-GBD, residues 230−288 of WASP which bind Cdc42Hs.

10.1021/bi992646d CCC: $19.00
Published on Web 03/16/2000

surface on Cdc42Hs may have important functional consequences. That is, a variety of effectors (e.g., PAK, ACK, WASP) and regulators (e.g., RhoGDI, Cdc42Hs-GAP) interact with the same binding surface on Cdc42Hs and the flexibility of portions of this surface may be required to form high affinity complexes with different binding partners.

EXPERIMENTAL PROCEDURES

Protein Expression. Cdc42Hs (1−178; as well as three amino acids (GSH) before the starting methionine) was expressed as a histidine-tagged protein in *Escherichia coli* [BL21(DE3)] from pET-15b-Cdc42Hs (*17*). $^{15}NH_4Cl$ and/or [^{13}C]glucose were substituted for unlabeled compounds in M9 media for the production of [^{15}N]- or [^{15}N,^{13}C]-Cdc42Hs (*17*). Fully deuterated [^{15}N]Cdc42Hs was produced as described previously (*17*) using [^{2}H]sodium acetate as the sole carbon source. The production of 70% deuterated [^{15}N,^{13}C]Cdc42Hs followed the procedure of Yamazaki et al. (*22*) using [^{13}C]glucose as the carbon source. PBD46 was expressed as a GST-fusion protein (pGEX-2T-PBD46) in *E. coli* [BL21(DE3)] as described previously (*17*).

Protein Purification. The purification of PBD46 and Cdc42Hs has been described in detail elsewhere (*17*). The exchange of GDP for GMPPCP was performed as described by John et al. (*23*). Following the exchange of nucleotide, PBD46 and Cdc42Hs were mixed in equimolar concentrations and incubated overnight at 4 °C. The complex was then purified on a Sephacryl S-100 column equilibrated with NMR buffer (25 mM NaCl, 5 mM NaH_2PO_4, 5 mM $MgCl_2$, and 1 mM NaN_3, pH 5.5, without pH correction to counter isotope effects). Samples were supplemented with 10% D_2O except for [^{1}H,^{13}C]NOESYHSQC, HCCHTOCSY, and [^{1}H,^{13}C]NOESY-purge experiments for which the sample was lyophilized and resuspended in 100% D_2O. The final concentrations of isotopically labeled Cdc42Hs·GMPPCP−PBD46 complexes ranged from 0.5 to 1 mM. As described previously (*17*), PBD46 bound with an affinity of 20 nM to Cdc42Hs and was found to be in slow exchange.

NMR Spectroscopy. All experiments were performed at 25 °C on a Varian Inova 600 Spectrometer with a triple resonance gradient probe at the Cornell Biomolecular NMR Center. Data were collected in States-TPPI mode (*24*, *25*) for quadrature detection, and chemical shifts were referenced as described previously (*16*).

2D Homonuclear and Heteronuclear Experiments. Homonuclear 2D NOESY (*26*) and TOCSY (*27*) spectra were acquired with presaturation during the recycle period followed by SCUBA recovery (*28*). A DIPSI-2 (*29*) mixing sequence of 50 ms was used in the TOCSY experiment, and a 100 ms mixing period, with an additional SCUBA recovery sequence, was used in the NOESY experiment. 2D [^{1}H,^{15}N]-HSQC and [^{1}H,^{13}C]HSQC (*30*) spectra were acquired using samples homogeneously labeled either on Cdc42Hs or PBD46 with ^{15}N or both ^{15}N and ^{13}C. Deuterium-exchange HSQCs were collected with 256 complex points in t_1 and 2048 in t_2 with spectral widths of 16 ppm in ω_2 and 59.2 ppm in ω_1 at intervals of 0.2, 0.5, 1, 3, 5.5, 8, and 23 h after resuspension in D_2O.

3D Experiments for Sequential Backbone Assignments. Complexes of Cdc42Hs·GMPPCP−PBD46 were prepared in which either Cdc42Hs or PBD46 was labeled with both ^{15}N and ^{13}C. For some experiments, Cdc42Hs was labeled to a level of 70% with ^{2}H in addition to ^{15}N and ^{13}C. HNCA spectra were collected using decoupling of C_β (*31*) as described by Yamazaki et al. (*22*) except for the removal of the sensitivity enhancement pulses. During t_1, WALTZ-16 decoupling was applied to protons, allowing the removal of T_c (C_α constant time period), and WURST decoupling (*32*, *33*) was applied to the C_β and carbonyl nuclei simultaneously (*31*). An HN(CO)CA experiment without sensitivity enhancement was used. This experiment was a modification of that described by Yamazaki et al. (*22*) except for the addition of SEDUCE decoupling of C_α nuclei during τ_c (in which coupling develops between the carbonyl and nitrogen), WURST decoupling of C_β nuclei in t_1, and WALTZ-16 decoupling of protons in t_1 (allowing the removal of T_c). In addition, HBCBCACONNH and HNCACB (*34*−*36*) experiments were used to correlate backbone amides and amide protons to C_β nuclei. In the case of the [^{2}H,^{15}N,^{13}C]Cdc42Hs·GMPPCP−PBD46 complex, HNCA, HN(CO)CA, HN(CO)-CACB, and HNCACB experiments were run with deuterium decoupling (*22*). An HNCO experiment was collected as described by Kay et al. (*37*) except for the omission of the selective water pulse and the substitution of SEDUCE decoupling of C_αs during nitrogen evolution with a 180° refocusing pulse.

3D Experiments for Side-Chain Assignments. [^{1}H,^{15}N]-TOCSYHSQC experiments were recorded using [^{15}N]-Cdc42Hs·GMPPCP−PBD46 and Cdc42Hs·GMPPCP-[^{15}N]-PBD46 with mixing times of 50 ms. HCCHTOCSY experiments were collected using [^{15}N,^{13}C]Cdc42Hs·GMPPCP−PBD46 and Cdc42Hs·GMPPCP-[^{15}N,^{13}C]PBD46 in 100% D_2O. The proton carrier was shifted upfield of the water resonance (2.37 ppm). HCCTOCSY and CCCTOCSY (*38*) experiments with deuterium decoupling were performed using the [^{2}H,^{15}N,^{13}C]Cdc42Hs·GMPPCP−PBD46 sample.

3D NOESY Experiments. [^{1}H,^{15}N]NOESYHSQC experiments (*25*, *39*) were acquired using [^{2}H,^{15}N]Cdc42Hs·GMPPCP−PBD46 (100% deuteration), [^{15}N]Cdc42Hs·GMPPCP−PBD46, and Cdc42Hs·GMPPCP-[^{15}N]PBD46. The pulse sequence includes water suppression by a selective pulse on the water resonance followed by dephasing with a gradient during the mixing period, as well as by a gradient applied while the magnetization of interest is spin-ordered during the final INEPT transfer step. A [^{1}H,^{13}C]NOESYHSQC experiment was acquired in 100% D_2O using the pulse sequence described above except that the selective water pulse was removed, nitrogen decoupling was added during the carbon chemical shift evolution period, and the proton carrier was shifted upfield of the water resonance (2.37 ppm).

Processing of NMR Experiments. Data were processed using a modification of version 2.3 of Felix software (Molecular Simulations, Inc.) on an SGI Indy computer. Preprocessing of sensitivity-enhanced experiments was performed as described by Kay et al. (*40*). Where necessary, the water resonance was reduced in the directly detected dimension by convolution of the FID with a sine-bell function of empirically determined width to identify the lowest frequency component, followed by its subtraction from the FID. Data were zero filled (typically to double the number of data points) and apodized by convolution with a squared sine-bell window function shifted by 70° (in most cases). Linear prediction was applied to the ω_1 dimension to increase

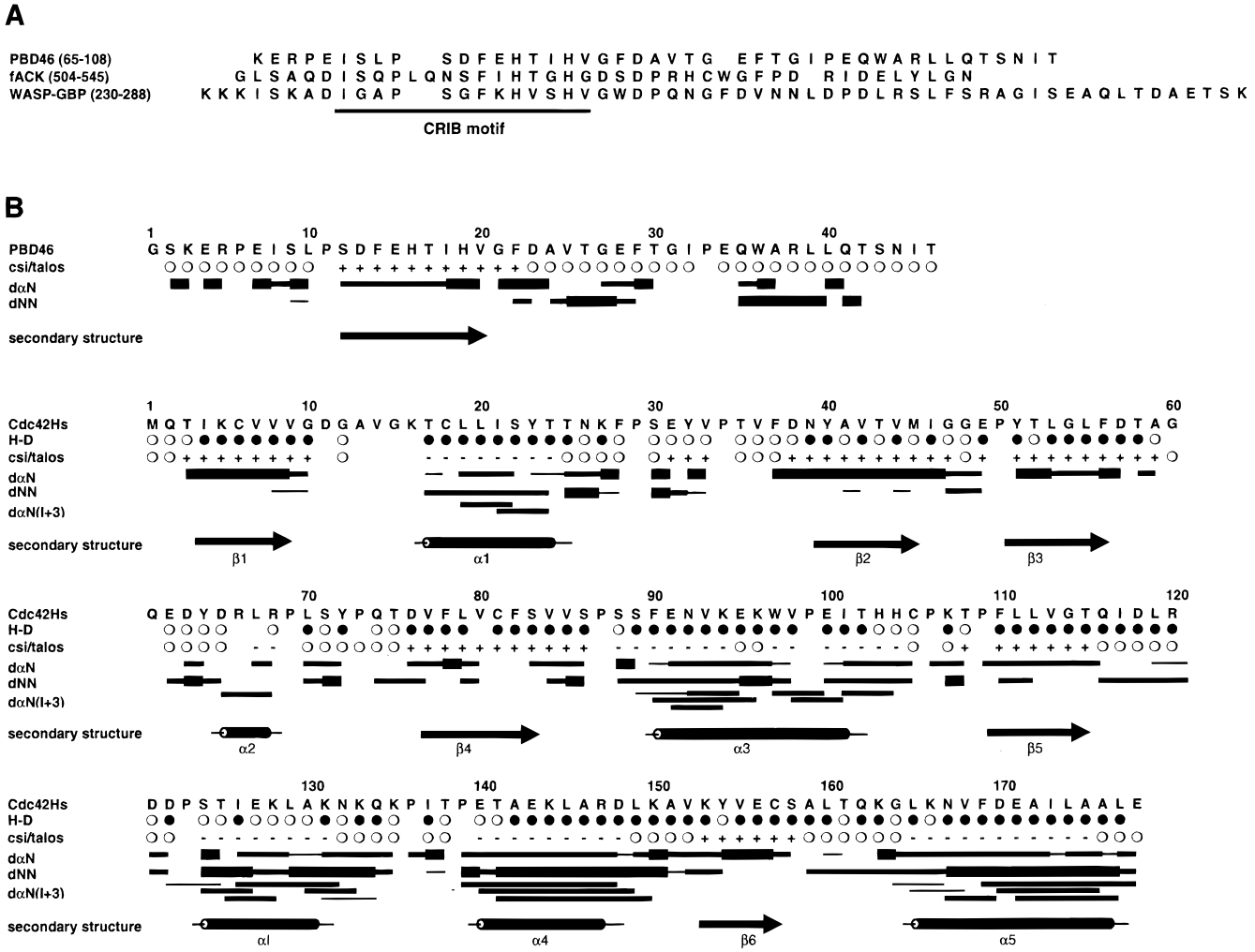

FIGURE 1: (A) Sequence alignment of PBD46 and the corresponding sequences from ACK and WASP. The CRIB sequence is underlined. Numbering shown is that for the intact protein. Note that PBD46 numbering throughout the text is relative to the peptide as indicated in Figure 1B. (B) Sequences of Cdc42Hs and PBD46 with the secondary structural elements indicated. Numbering for PBD46 is relative to the peptide rather than full-length PAK. Peptide numbering is used throughout the text. Also included are the deuterium exchange data [(○) rapid exchange of hydrogen for deuterium (i.e., less than 15 m), and (●) protection from exchange for more than 30 m]; the chemical shift index from Wishart analysis (*43*, *44*) and TALOS (*42*) [(−) correlated with helix, (+) with β-strand, and (○) with coil] and NOE constraints between the indicated backbone atoms.

resolution in 3D experiments. In the case of 3D NOESY experiments, linear prediction was applied in both indirectly determined dimensions. The XEASY program was used for data visualization and assignments (*41*) and PEAKINT (N. Schäfer, diploma thesis, ETH, Zürich, Switzerland) was used for integration of the NOESY spectra. TALOS (*42*) and the chemical shift index (*43*, *44*) were used to calculate dihedral restraints from chemical shift data.

Structure Calculation. Distance constraints for structure calculations were obtained from [^{1}H,^{15}N]- and [^{1}H,^{13}C]-NOESYHSQC experiments. Constraints for the interface between Cdc42Hs and PBD46 were derived from a [^{1}H,^{15}N]-NOESYHSQC experiment in which Cdc42Hs was ^{15}N-labeled and fully deuterated and from [^{1}H,^{13}C]NOESYHSQC experiments with a purge pulse (either Cdc42Hs or PBD46 was ^{13}C-labeled) to select NOEs between protons bound to ^{12}C and those bond to ^{13}C (*45*). Approximately 1900 constraints from NOESY spectra (74 intermolecular and 1812 intramolecular) were classified into five categories according to the relative strength of the NOESY cross-peak (<2.4, <2.9, <3.4, <4.0, and <5.5 Å). As indicated by the secondary structures, deuterium exchange rates, chemical shift indices, and characteristic NOE patterns (Figure 1), 55 hydrogen bonds were included. For each hydrogen bond, the carbonyl oxygen to amide proton distance was constrained to 1.8−3.0 Å and the carbonyl oxygen to amide nitrogen distance was constrained to 2.5−4.0 Å. On the basis of the chemical shift indices (*43*, *44*) and characteristic NOE patterns, backbone dihedral angles of residues in α-helices and β-strands were loosely constrained to favorable regions of ϕ,ψ space: α-helix, ϕ, $-80 \pm 30°$; ψ, $-20 \pm 30°$; β-strand, $-105 \pm 65°$; ψ, $-145 \pm 45°$ (*46*). Additionally, based on TALOS (*42*), ϕ,ψ angles were constrained to the maximum of three times the standard deviation or ±30°.

The 2412 distance and dihedral restraints were used to produce preliminary structures with XPLOR 3.851 (*47*). Substructures containing only N, HN, H_α, C_α, C′, C_β, and C_γ atoms were calculated using metric matrix distance geometry. The missing atoms were then included, and the structures were refined using simulated annealing and energy minimization using center averaging to represent constraints to nonstereospecifically assigned atoms and a square well potential to hold constrained atoms together. A second step of simulated annealing and energy minimization included

the dihedral angle restraints derived from chemical shifts using TALOS (*42*). The final step included "Ramachandran refinement" to constrain the dihedral angles to those that are known to be physically realizable (*48*). The 20 best structures were selected on the basis of low overall energy and constraint violations. Because of the paucity of NOEs observed between Cdc42Hs and GMPPCP, the nucleotide was modeled into the structure based on homology with the structure of Cdc42Hs in complex with fACK (*21*). The lack of NOEs between GMPPCP and Cdc42Hs is likely due in part to unfavorable dynamics in this region of the protein and the fact that the native protein was used rather than the Q61L mutant [a mutant which abolishes GTP hydrolysis (*21*)]. Structures were visualized using Insight II (Molecular Simulations, Inc.) and MOLMOL (*49*), and were analyzed using PROCHECK (*46*) and NMRCLUST (*50*).

RESULTS AND DISCUSSION

Sequential Assignments of PBD46. Previous fluorescence and NMR experiments have demonstrated that the complex between PBD46 and Cdc42Hs is in slow exchange with a K_D of approximately 20 nM (*17*). Because of the high affinity of the complex, it could be purified as a 1:1 complex by gel filtration and only one set of bound peaks were observed in a [^{1}H,^{15}N]HSQC spectrum (*17*).

Backbone assignments were done using a combination of triple resonance (Cdc42Hs·GMPPCP-[^{15}N,^{13}C]PBD46), double resonance (Cdc42Hs·GMPPCP-[^{15}N]PBD46), and homonuclear experiments ([^{2}H,^{15}N]Cdc42Hs·GMPPCP−PBD46). The HNCA and HN(CO)CA experiments provide correlations between a given amide proton and nitrogen and both the $C_{\alpha i}$ and $C_{\alpha(i-1)}$ and allowed the unambiguous sequential backbone assignments in most cases. For a few residues, the sequential assignment using HNCA and HN(CO)CA was complicated by overlap in the C_α chemical shifts. In these cases, additional information from the three-dimensional NOESYHSQC and TOCSYHSQC were used to aid in the selection of the correct neighbor. In addition, the HNCACB correlates the amide proton and nitrogen and both the $C_{\beta i}$ and $C_{\beta(i-1)}$, while the HBCBCACONNH correlates the amide proton and nitrogen and the interresidue $C_{\alpha(i-1)}$ and $C_{\beta(i-1)}$. These experiments aided the sequential assignment and provided the assignment of the C_βs. The two-dimensional TOCSY and NOESY spectra of PBD46 complexed with fully deuterated Cdc42Hs were also used to confirm some of the chemical shift assignments. Backbone resonances from 96% of the nonproline residues were assigned.

Side-chain assignments were achieved using 3D [^{1}H,^{15}N]-TOCSYHSQC and HCCHTOCSY experiments. Most of the H_α and H_β resonances and a portion of the H_γ atoms were assigned using the [^{1}H,^{15}N]TOCSYHSQC spectrum collected with a 50 ms mixing time. Additional side-chain resonances were assigned using the HCCHTOCSY spectrum, which was particularly useful for residues with long side chains such as Ile, Leu, Arg, and Lys. Side-chain resonances from 95% of the amino acids were assigned.

Sequential Assignments of Cdc42Hs. Backbone assignments of Cdc42Hs were obtained using a combination of three-dimensional, deuterium-decoupled HNCA, HNCACB, HNCOCA, and HN(CO)CACB spectra using 70% deuterated [^{13}C,^{15}N]Cdc42Hs·GMPPCP complexed to natural abundance PBD46. In some cases, the 3D [^{1}H,^{15}N]TOCSYHSQC and [^{1}H,^{15}N]NOESYHSQC experiments ([^{15}N]Cdc42Hs·GMPPCP PBD46) were used to confirm assignments. Using this approach, backbone resonances from 96% of the nonproline residues were assigned. Side-chain assignments were made with the [^{13}C,^{15}N]Cdc42Hs·GMPPCP−PBD46 sample in the case of the HCCH-TOCSY and the 70% deuterated [^{13}C,^{15}N]-Cdc42Hs·GMPPCP−PBD46 sample in the case of the CCC-TOCSY and HCCTOCSY experiments. The [^{1}H,^{15}N]TOC-SYHSQC and [^{1}H,^{15}N]NOESYHSQC experiments were used in some cases to confirm assignments. Side-chain resonances from 87% of the amino acids were assigned.

Intermolecular Chemical Shift Assignments of the Cdc42Hs·GMPPCP−PBD46 Complex. A fully deuterated [^{15}N]-Cdc42Hs·GMPPCP sample was purified in H_2O-containing buffers and complexed with natural abundance PBD46. During the purification procedure, protons were exchanged back onto the amides, providing a Cdc42Hs sample with protons on the amides and deuterons on the carbons. A three-dimensional [^{1}H,^{15}N]NOESYHSQC spectrum was used to detect the NOE interactions between the amide protons within Cdc42Hs and intermolecular interactions between Cdc42Hs and PBD46. Since the carbon nuclei of the Cdc42Hs are deuterated, cross-peaks that are observed in the C_α region and further upfield (approximately 5 to −1 ppm) are due to intermolecular NOE interactions between Cdc42Hs and PBD46. In some cases, intermolecular NOE interactions between some amide protons could be assigned without ambiguity. Another strategy for detecting intermolecular interactions employed a pulsed field gradient three-dimensional isotope-filtered [^{1}H,^{13}C]NOESYHSQC experiment (*45*) with purge pulses designed to observe selectively interactions between protons bound to ^{13}C and those bound to ^{12}C. Both [^{15}N,^{13}C]Cdc42Hs·GMPPCP bound to natural abundance PBD46 and [^{15}N,^{13}C]PBD46 bound to natural abundance Cdc42Hs were used. This experiment can resolve ambiguities between intra- and intermolecular NOEs in the three-dimensional [^{1}H,^{13}C]NOESYHSQC spectrum of the complex and provided the identification of the intermolecular cross-peaks between side chain and the C_α protons of the PBD46 and Cdc42Hs.

Overall structure of the Cdc42Hs·GMPPCP−PBD46 Complex. A set of 20 superimposed structures of the Cdc42Hs·GMPPCP−PBD46 complex is shown in Figure 2B. The structure is well resolved (rms deviation of 0.63 ± 0.14 Å for the core (*50*) of the structure and 1.11 ± 0.18 Å for the secondary structure; Table 1) except for portions of switch I and switch II which are known from measurements of backbone dynamics to exhibit additional flexibility (*19*). Consistent with the solution structure of Cdc42Hs·GDP (*16*), Cdc42Hs in complex with PBD46 consists of a central six-stranded β-sheet which is curled about the axis of helix α5 (Figure 2A). Two other helices, α3 and α4, flank the convex surface formed by the β-sheet, and helix α1 lies perpendicular to the β-strands on the concave side of the sheet. However, there are notable differences between the unbound structures of Cdc42Hs (*16*, *21*) and the structure of the protein bound to PBD46. A number of resonances in switch I and switch II that could not be assigned in either the GDP or GMPPCP-bound forms (*16*, *21*) could easily be detected in the complex with PBD46 (*17*). This may be a result, at least in part, of stabilization of the backbone dynamics of

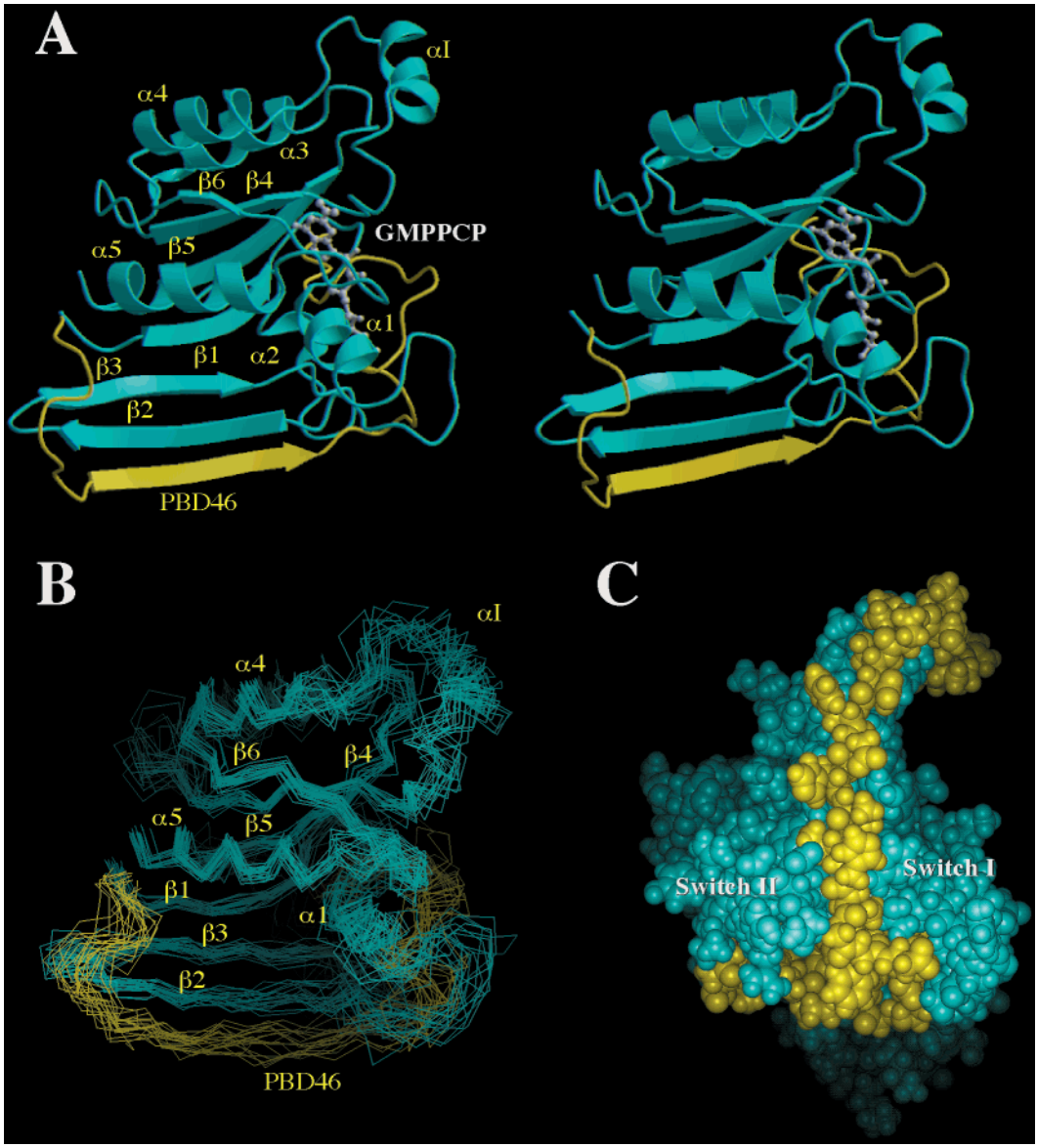

FIGURE 2: (A) Most representative structure (*64*) of the Cdc42Hs·GMPPCP complex with PBD46 is presented as a stereo representation. GMPPCP is shown as a ball-and-stick representation in white. This figure was produced using MOLSCRIPT (*65*) and Raster3D (*66*). (B) The superimposition of 20 structures of the complex between Cdc42Hs·GMPPCP and PBD46. Traces through the Cα atoms are shown. Cdc42Hs is shown in cyan and PBD46 is in yellow. (C) CPK representation of the Cdc42Hs·GMPPCP PBD46 complex illustrating the binding interface and the positioning of switch I and switch II on either side of PBD46. Cdc42Hs is shown in cyan and PBD46 is in yellow.

Cdc42Hs upon binding PBD46 (*19*). PBD46 extends the β sheet of Cdc42Hs by adopting a β-strand antiparallel to β2 of Cdc42Hs. However, the amide protons in the β2 strand of Cdc42Hs which contact PBD46 are not protected from H−D exchange (Figure 1). This is most likely due to the fact that the rate constant for PBD46 dissociation is approximately 0.7 s^{-1} (*51*), which is fast relative to the successive HSQC experiments used in the measurement of H−D exchange. Both β2 and the corresponding strand in PBD46 are somewhat less well-defined than the remainder of the β sheet. Although the complex is in slow exchange, the intermolecular interactions between Cdc42Hs and PBD46 are clearly less stable than the intramolecular interactions within Cdc42Hs. In the absence of PBD46, the portion of the β-sheet formed by β2 and β3 exhibits a twist near the tip of the loop between β2 and β3. Upon binding PBD46, the region is flattened somewhat and PBD46 loops behind the sheet to interact with α5 (Figure 2A). Like the GDP-bound form of Cdc42Hs (*16*), the amide protons of the helix in the insert region (α_I) exhibit fast H−D exchange (with the exception of I126). Apparently, both in the bound and unbound forms of Cdc42Hs, this helix is less stable than the other elements of secondary structure. Previous studies of the backbone dynamics (*19*) suggested that α3 exhibits some mobility relative to the molecular frame. Consistent with this, we have found that a subpopulation of structures exhibit approximately a 60° rotation around the long axis of the helix. Only the major conformer is shown in Figure 2.

The α1 helix is reoriented by approximately 90° to accommodate PBD46. Switch II of the Cdc42Hs−PBD46 complex contains a short helix (α2; Figure 2A). This helix was not observable in the Cdc42Hs·GDP solution structure (*16*) but was seen in the crystal structure of Cdc42Hs·GDP (N. Nassar and R. A. Cerione, unpublished observations). Studies of the backbone dynamics of this region of the protein are consistent with low-amplitude motion on the

Table 1: Structural Statistics

	ensemble of 20 structures	most representative structure[a]
coordinate precision[b]		
RMSD over core (Å)[c]	0.63 ± 0.14	0.38
RMSD over secondary structure (Å)	1.11 ± 0.18	0.80
statistics for structure calculation		
RMSD from experimental restraints		
NOE distances (Å)	0.056 ± 0.003	0.047
dihedral angles (deg)	0.86 ± 0.12	0.834
RMSD over secondary structure		
bonds (Å)	0.004 ± 0.0002	0.004
angles (deg)	0.73 ± 0.02	0.71
impropers (deg)	0.56 ± 0.02	0.54
procheck analysis		
most favored (%)	66 ± 2	66
additional allowed (%)	27 ± 2	28
generously allowed (%)	6 ± 2	6
disallowed region (%)	0.9 ± 0.7	0
overall *G*-factor[d]	−0.44 ± 0.02	−0.42

[a] The most representative structure determined by NMRCLUST (*64*) and is that structure shown in Figures 2 and 3. [b] Determined relative to the average structure calculated by XPLOR (*47*). [c] The core of the structure was defined using NMRCORE (*50*) to be residues 4−9, 51−56, 77−83, 110−115, and 153−157. [d] Ideally, the *G*-factor should be greater than −0.5. Values less than −1.0 imply structural problems.

nanosecond time scale and chemical exchange on the millisecond time scale in the GDP- and GMPPCP-bound forms of the protein, and the binding of PBD46 significantly reduces the motion in switch II (*19*).

The N-terminus of PBD46 interacts largely with the C-terminus of Cdc42Hs. Interactions are also observed between PBD46 and α1, switch I and switch II of Cdc42Hs. Both switch I and II are mobile in the unbound protein, but flank PBD46 in the bound structure (Figure 2C). However, there are no interactions observed between PBD46 and the insert region of Cdc42Hs. As shown in Figure 2A, PBD46 generally adopts an extended structure encompassing large areas of Cdc42Hs, consistent with distribution of intermolecular NOEs across the surface of Cdc42Hs. The N-terminus of the peptide bends at residue I8, allowing interactions with the C-terminus of Cdc42Hs. It also forms a turn at residue G21 and a loop between residues G27 and W36, with the remaining C-terminal residues in an extended conformation with few interactions with Cdc42Hs. Approximately 17% of the surface of Cdc42Hs is buried upon binding PBD46 (1940 ± 120 Å^2).

Interface between PBD46 and Cdc42Hs. PAK, WASP, and ACK can all act as downstream effectors of Cdc42Hs and have a sequence motif known as the CRIB (Cdc42/Rac interactive binding) domain which was previously identified as the site of interaction with Cdc42Hs and Rac (*15*). Our previous work (*17*) identified the major sites of interaction on Cdc42Hs which bind PAK, and this binding surface is, for the most part, common to the complex of Cdc42Hs with WASP-GBD and fACK (*20, 21*). With the availability of NMR structures of complexes between Cdc42Hs and peptides derived from three of its effectors, it is possible to investigate the specific interactions which are responsible for the specificities of each of these kinases.

Prior to binding, both fACK (*21*) and PBD46 (*51*) are unstructured as is evident from 2D homonuclear NOESY and 3D [^{1}H,^{15}N]NOESY−HSQC spectra; whereas, WASP-GBD exhibits an α-helical structure near the C-terminus (*20*). The complex of Cdc42Hs·GMPPCP with PBD46 is very similar to the complex with fACK (with the exception of several interesting differences described below) and differs in many aspects from the complex with WASP-GBD.

Interaction of the N-Terminal Portion of PBD46 with β2 and the C-Terminus (α5) of Cdc42Hs. As identified previously, the β2 strand of Cdc42Hs forms an antiparallel intermolecular extension of the Cdc42Hs β-sheet with residues S12 to F19 of PBD46 (Figures 2A and 3A). This is similar to the extension of the β-sheet in Rap1a/Raf-1 complex, although the extent of the binding surface between Cdc42Hs and PBD46 is much greater than that observed for the Rap1a/Raf-1 complex (*18*). Both WASP and ACK are specific to Cdc42Hs; whereas, PAK binds both Cdc42Hs and Rac1. Site-directed mutagenesis has implicated V42 and L174 of Cdc42Hs in determining the specificity of these effectors (the corresponding positions in Rac1 are alanine and arginine). Mutation of either V42 or L174 to alanine significantly reduced fACK binding, but only the mutation of L174 affected the binding of a peptide derived from WASP (*21*). Binding of a PAK peptide was only reduced by a factor of 2 for each mutation. The NMR structure of the Cdc42Hs−fACK complex indicates that V42 in β2 of Cdc42Hs exhibits a hydrophobic interaction with I519 in fACK and that L174 packs against L505 of fACK. The NMR structure of Cdc42Hs-WASP-GBD (*20*) shows the interactions of L174 with a number of hydrophobic residues in WASP-GBD, suggesting a significant contribution to the binding energy. In PBD46, the residue equivalent to I519 in fACK is glutamate (E15) and the residue equivalent to L505 in fACK is lysine (K3). We observed NOEs between the H_γ of V42 (Cdc42Hs) and H_β of E15 (PBD46). NOEs were also observed between V42 of Cdc42Hs and the conserved CRIB residue, F14 (PBD46). This implies that, like the hydrophobic interactions between I519 and V42 in Cdc42Hs−fACK complex, the Cdc42Hs·GMPPCP−PBD46 interaction is stabilized by hydrophobic interactions. In addition, the binding energy is enhanced by the interaction of the carboxylate group of E15 (PBD46) with the hydroxyl group of Y40 (Cdc42Hs). This interaction would not be present in fACK in which the corresponding residue is an isoleucine or WASP where the corresponding position is lysine. Also, the aromatic ring of Y40 (Cdc42Hs) makes hydrophobic contacts with T17 and E15 of PBD46 (Figure 3C). The interactions of Y40 (Cdc42Hs) with PBD46 are likely to be the reason the mutation of V42 to A in Cdc42Hs does not have significant effect on the binding of PAK (Figure 3C), but that the Y40C mutation of the constitutively active Q61L mutant of Cdc42Hs abolishes the binding of p65^{PAK} (*52*). The conservation of Y40 in Rac1 may at least partially explain why PAK can interact with both Cdc42Hs and Rac1. The hydrophobic portion of K3 (PBD46) packs into a hydrophobic pocket consisting of L174, L177, and perhaps part of the hydrophobic portion of the E178 side chain (Cdc42Hs; Figure 3D). The interaction of the hydrophobic portions of K3 with this hydrophobic pocket (in particular L177) may be the dominant binding interactions in this portion of the interface, explaining why the mutation of L174 to A of Cdc42Hs has only a modest effect on the binding of PAK. As shown previously (*17*), the removal of K3, E4, and R5 from PBD46 resulted in a decrease in the affinity of

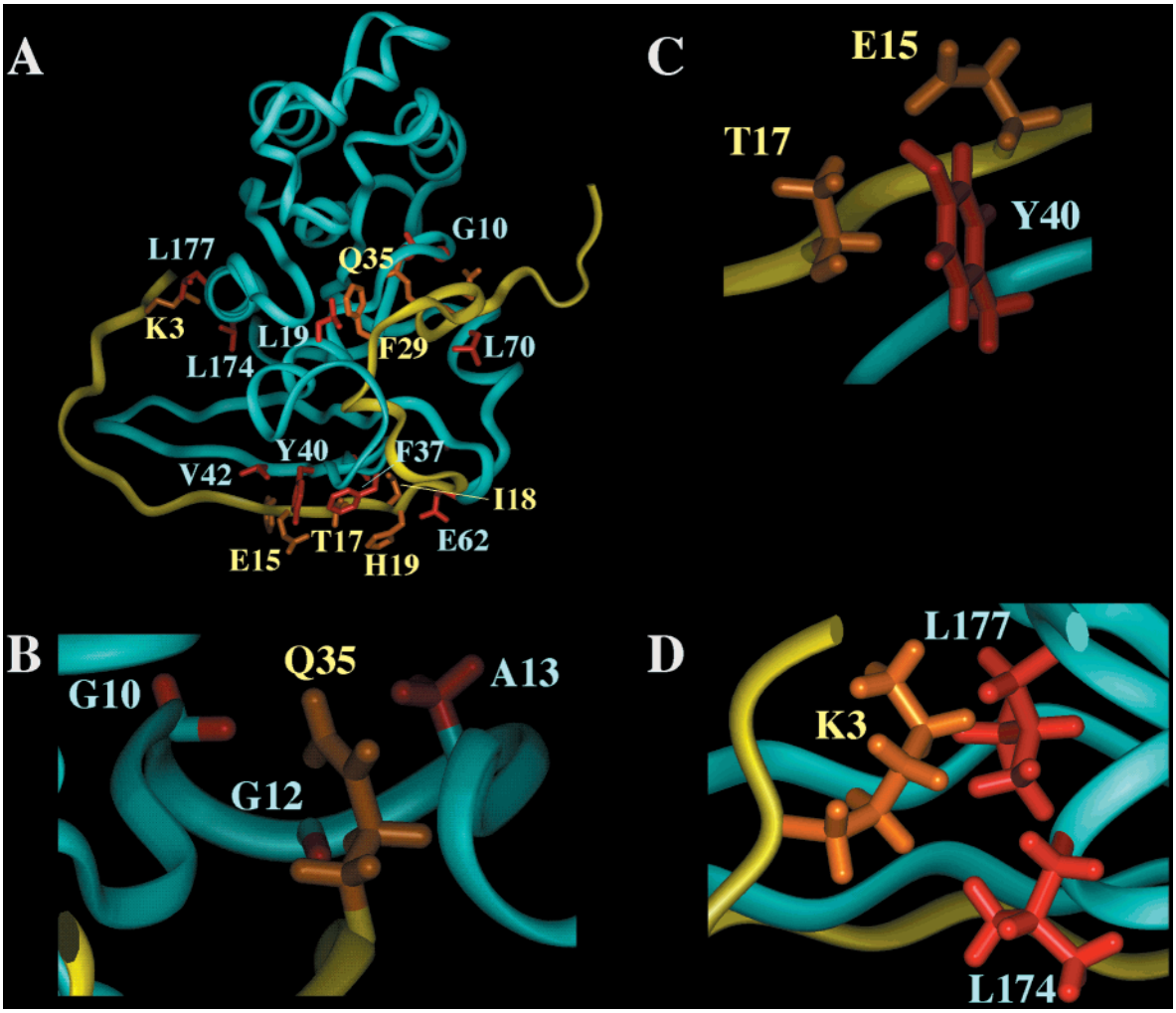

FIGURE 3: Structure of Cdc42Hs/PBD46 interface. In all four panels, the backbone of Cdc42Hs is shown in cyan and that of PBD46 is shown in yellow. Side chains of Cdc42Hs are shown in red, and side chains of PBD46 are shown in orange. (A) A ribbon representation illustrating a number of the important interactions between Cdc42Hs and PBD46. (B) The interaction between the Q35 (PBD46) and G10, G12, and A13 of Cdc42Hs. (C) Both T17 and E15 (PBD46) make hydrophobic interactions with Y40 (Cdc42Hs). In addition, the carboxyl group of E15 (PBD46) can hydrogen bond with the hydroxyl of Y40 (Cdc42Hs). (D) The methylenes of K3 (PBD46) interact with a hydrophobic pocket made up of L174 and L177 (Cdc42Hs).

the PBD46 to Cdc42Hs by approximately 50-fold, suggesting the importance of this portion of PBD46 to the binding energy (mainly via K3). Interestingly, position 174 is an arginine in Rac1, suggesting the possibility that E4 of PBD46 could interact with this position in the Rac1−PBD46 complex. Residues I46 and L177 in Cdc42Hs pack against residue I510 in fACK (the first residue in the CRIB consensus sequence) but these interactions have not been observed in Cdc42Hs−PBD46.

Stevens et al. (*53*) have used the transferred NOESY technique to determine the structure of the PAK-2 CRIB sequence (22 amino acids) bound to Cdc42Hs. They observed a loop conformation around residues F14, H16, I18, H19, and V20 (PBD46 numbering), but both the N- and C-termini of the PAK-2 CRIB structure were not well-defined. This loop conformation and the orientation of the side chains differ somewhat from the Cdc42Hs−PBD46 complex shown in Figure 3A. Instead of the loop conformation, the PBD46 has an extended conformation even beyond the residues mentioned above, embracing a large surface area of Cdc42Hs. In addition, several side-chain orientations are different in the Cdc42Hs·GMPPCP−PBD46 structure vs the CRIB structure. For example, H19 (PBD46), rather than forming a portion of a "hydrophobic cluster" seen in the PAK-2 CRIB structure, points away from the interface to make contacts with F37 (Cdc42Hs). I18 (PBD46) makes hydrophobic contacts with N39, A59, and E62 (Cdc42Hs) and orients toward the interface instead of outward as observed in the PAK-2 CRIB structure. Furthermore, both binding assays using peptides derived from PAK (*17*) and the Cdc42Hs−PBD46 structure (described above) demonstrate the significance of the N-terminus in the binding interaction. The 22 amino acid PAK-2 CRIB peptide lacks K3 and E4 (PBD46) in the N-terminus (although they are present in wild-type protein) and has a much lower affinity for Cdc42Hs than both PBD46 and wild-type PAK.

Interaction of PBD46 with α1, Switch I, and Switch II of Cdc42Hs. Both switch I and switch II exhibit considerable flexibility in the GDP- and GMPPCP-bound forms of Cdc42Hs and become considerably more rigid upon binding PBD46 (*19*). In fact, in the absence of PBD46, several residues are not observable in the NMR spectrum but become detectable upon binding PBD46, consistent with a change in backbone dynamics (*17*, *19*). Likewise, switch I and switch

II regions of Cdc42Hs were found to be observable in the Cdc42Hs−fACK and Cdc42Hs−WASP-GBD complexes. A number of interactions are observed between residues in the switch I region and PBD46. T35 (Cdc42Hs) makes hydrophobic contacts with A24 and V25 (PBD46). The F37A mutant of the Cdc42Hs has no effect on the interaction with PAK (*52*). However, as shown in Figure 3A, F37 makes hydrophobic contacts with H19 of PBD46, and F37 points toward the interface instead of away from the binding site of PBD46 as was previously predicted (*17*). Presumably, the interactions with F37 do not contribute extensively to the enthalpy of binding. As mentioned above (Figure 3C), Y40 (Cdc42Hs) interacts with both E15 and T17 (PBD46). In switch II, E62 (Cdc42Hs) packs against I18 of PBD46, and L70 (Cdc42Hs) interacts with A37 (PBD46). The α1 helix is reoriented and packs against PBD46, facilitating the interaction of L19 (Cdc42Hs) with F29 (PBD46). In the adjoining P-loop of Cdc42Hs, residues G10, G12, and A13 interact with E34 and Q35 of PBD46 (Figure 3B). These interactions may be particularly important for the inhibition of the rate of hydrolysis of GTP upon PBD46 (and PAK) binding.

Structure−Function. The large binding surface between PBD46 and Cdc42Hs is interesting for a number of reasons. The points of contact encompass the homologous binding surface of the Rap1a/Raf-1 complex (*18*) but, in addition, include switch I, switch II, the P-loop, α1, and α5. This larger binding surface (in particular the interactions with the P-loop) is consistent with the effects of PBD46 on both the GDP-GTP exchange rate and the rate of GTP hydrolysis (*17*). In contrast, Raf-1 has no effect on the rate of nucleotide hydrolysis of Rap1a. The reorientation of α1 occurs in both the Cdc42Hs·GMPPCP−PBD46 (Figure 2A) and Cdc42Hs·GMPPNP-fACK (*21*) complexes but was not observed in Cdc42Hs·GMPPCP−WASP-GBD (*20*) complex. Crystal structures of Ras·GDP (*54*), Ras·GMPPNP (*55*), and Cdc42Hs·GDP (N. Nassar and R. A. Cerione, unpublished observations) have shown that residues in α1 such as K16, S17, and A18 interact directly with the nucleotide. In both Cdc42Hs (*56*) and H-Ras (*57*), mutations in the P-loop (e.g., G12V) inhibit GTP hydrolysis. Presumably, the inhibition of GTP hydrolysis is due to a perturbation of the conformation of Q61 (*58*, *59*). The differences in the structures of Cdc42Hs when bound to the different effectors may provide clues to their differential effects on the rate of GTP hydrolysis. PBD46 significantly decreases the rate of GTP hydrolysis when bound to Cdc42Hs (*17*, *60*). The half-life of GTP bound to Cdc42Hs increases from 8.6 min to greater than 40 min in the presence of PBD46, whereas fACK increased the half-life of GTP from 6.5 to 10 min (*11*). One potential explanation for the large effect of PBD46 on GTP hydrolysis is that PBD46 makes more extensive contacts with switch I than does ACK, which may restrict the available conformations. The reorientation of α1 together with other specific interactions between residues in both α1 and switch I and PBD46 are likely to be responsible for the effects of PBD46 on the rate of GTP hydrolysis by Cdc42Hs.

The binding surface includes portions of switch I and switch II that are at least partially disordered in the unbound forms of Cdc42Hs (*19*). Likewise, PBD46 is completely unstructured in the free state (*51*). Upon binding, the backbone dynamics of Cdc42Hs are significantly reduced and PBD46 assumes an ordered conformation. Thus, at least in terms of the protein backbone, the binding event involves a loss of entropy. Indeed, isothermal titration microcalorimetry has shown that binding is driven by the increase in enthalpy at the expense of a decrease in entropy (*51*). GAP (*61*, *62*), GDI (*63*), WASP-GBD (*20*), fACK (*21*), and PBD46 all bind to the face of Cdc42Hs, termed the "switch surface" (*16*), which includes switch I, switch II, and other residues that are affected by the state of the nucleotide. The partially disordered conformations of the unbound states may have important functional consequences in that a well ordered structure might not be capable of making contacts with such a wide variety of signaling proteins. The backbone flexibility may, therefore, be necessary to form tight, enthalpy-driven interactions and also to accommodate interactions with a variety of effectors and regulators.

Summary. PBD46 makes extensive contacts with Cdc42Hs, covering an area which includes much of the surface that is affected when Cdc42Hs is activated by the exchange of GDP for GTP. The binding is accompanied by conformational changes, most notably a reorientation of helix α1, and changes in backbone dynamics in both PBD46 and Cdc42Hs. The extensive binding surface, encompassing many of the residues that contact the nucleotide, and the rotation of α1 are consistent with the effects of PBD46 on GTP hydrolysis by Cdc42Hs. Also, the fact that the binding interface on Cdc42Hs is partially disordered in the unbound state is likely to have important functional consequences in that it can accommodate a wide variety of effectors and regulators.

ACKNOWLEDGMENT

We are grateful to the Laboratory of Chemical Physics at the National Institutes of Health and Dr. Frank Delaglio for making available the program TALOS and to Drs. Lewis Kay (University of Toronto) and Gerhard Wagner (Harvard Medical School) for many of the pulse sequences that were used. We thank Adrienne Loh (University of Wisconsin, La Crosse), Raymond Vazquez, Linda Nicholson, Joanna Feltham (University of Massachusetts), Gregory Weiland, Richard Cerione, Nicholas Nassar, Volker Dötsch (University of California, San Francisco), and Gerhard Wagner (Harvard Medical School) for helpful discussions. This research was conducted using the resources of the Cornell Theory Center, which receives funding from Cornell University, New York State, federal agencies, and corporate partners.

REFERENCES

1. Bourne, H. R., Sanders, D. A., and McCormick, F. (1991) *Nature 349*, 117−127.
2. Martin, G. A., Bollag, G., McCormick, F., and Abo, A. (1995) *EMBO J. 14*, 1970−1978.
3. Minden, A., Lin, A., Claret, F. X., Abo, A., and Karin, M. (1995) *Cell 81*, 1147−1157.
4. Zhang, S., Han, J., Sells, M. A., Chernoff, J., Knaus, U. G., Ulevitch, R. J., and Bokoch, G. M. (1995) *J. Biol. Chem. 270*, 23934−23936.
5. Bagrodia, S., Derigard, B., Davis, R. J., and Cerione, R. A. (1995) *J. Biol. Chem. 270*, 27995−27998.
6. Ridley, A. J., Paterson, H. F., Johnston, C. L., Diekmann, D., and Hall, A. (1992) *Cell 70*, 401−410.
7. Vojtek, A. B., and Cooper, J. A. (1995) *Cell 82*, 527−529.
8. Chant, J., and Stowers, L. (1995) *Cell 81*, 1−4.

9. Zheng, Y., Bagrodia, S., and Cerione, R. A. (1994) *J. Biol. Chem. 269*, 18727−18730.
10. Aspenstrom, P., Lindberg, U., and Hall, A. (1996) *Curr. Biol. 6*, 70−75.
11. Manser, E., Leung, T., Salihuddin, H., Tan, L., and Lim, L. (1993) *Nature 363*, 364−367.
12. Yang, W., and Cerione, R. A. (1997) *J. Biol. Chem. 222*, 24819−24824.
13. Bagrodia, S., Taylor, S., Creasy, C., Chernoff, J., and Cerione, R. (1995) *J. Biol. Chem. 270*, 22731−22737.
14. Manser, E., Leung, T., Salihuddin, H., Zhao, Z., and Lim, L. (1994) *Nature 367*, 40−46.
15. Burbelo, P. D., Drechsel, D., and Hall, A. (1995) *J. Biol. Chem. 270*, 29071−29074.
16. Feltham, J. L., Dötsch, V., Raza, S., Manor, D., Cerione, R. A., Sutcliffe, M. J., Wagner, G., and Oswald, R. E. (1997) *Biochemistry 36*, 8755−8766.
17. Guo, W., Sutcliffe, M. J., Cerione, R. A., and Oswald, R. E. (1998) *Biochemistry 37*, 14030−14037.
18. Nassar, N., Horn, G., Herrmann, C., Scherer, A., McCormick, F., and Wittinghofer, A. (1995) *Nature 375*, 554−560.
19. Loh, A. P., Guo, W., Nicholson, L. K., and Oswald, R. E. (1999) *Biochemistry 39*, 12547−12557.
20. Abdul-Manan, N., Aghazadeh, B., Liu, G. A., Majumdar, A., Ouefelli, O., Siminovich, K. A., and Rosen, M. K. (1999) *Nature 399*, 379−383.
21. Mott, H. R., Owen, D., Nietlispach, D., Lowe, P. N., Manser, E., Lim, L., and Laue, E. D. (1999) *Nature 399*, 384−8.
22. Yamazaki, T., Lee, W., Arrowsmith, C. H., Muhandiram, D. R., and Kay, L. E. (1994) *J. Am. Chem. Soc. 116*, 11655−11666.
23. John, J., Sohmen, R., Feurstein, J., Linke, R., Wittinghofer, A., and Goody, R. S. (1990) *Biochemistry 29*, 6058−6065.
24. States, D. J., Haberkorn, R. A., and Ruben, D. J. (1982) *J. Magn. Reson. 48*, 286−292.
25. Marion, D., Driscoll, P. C., Kay, L. E., Wingfield, P. T., Bax, A., Gronenborn, A., and Clore, G. M. (1989) *Biochemistry 28*, 6150−6156.
26. Braunschweiler, L., and Ernst, R. R. (1983) *J. Magn. Reson. 53*, 521−528.
27. Kumar, A., Ernst, R. R., and Wüthrich, K. (1980) *Biochem. Biophys. Res. Commun. 95*, 1−6.
28. Brown, S. C., Weber, P. L., and Mueller, L. (1988) *J. Magn. Reson. 77*, 166−169.
29. Rucker, S. P., and Shaka, A. J. (1989) *Mol. Phys. 68*, 509−517.
30. Bodenhausen, G., and Ruben, D. J. (1980) *Chem. Phys. Lett. 69*, 185−189.
31. Matsuo, H., Kupce, E., Li, H., and Wagner, G. (1996) *J. Magn. Reson., Ser. B 113*, 91.
32. Kupce, E., and Wagner, G. (1995) *J. Magn. Reson., Ser. B 109*, 329.
33. Kupce, E., and Freeman, R. (1996) *J. Magn. Reson., Ser. A 118*, 299.
34. Muhandiram, D. R., and Kay, L. E. (1994) *J. Magn. Reson. 103*, 203−216.
35. Grzesiek, S., and Bax, A. (1992) *J. Am. Chem. Soc. 114*, 6291−6293.
36. Grzesiek, S., and Bax, A. (1992) *J. Magn. Reson. 99*, 201−207.
37. Kay, L. E., Xu, G. Y., and Yamazaki, T. (1994) *J. Magn. Reson., Ser. A 109*, 129−133.
38. Grzesiek, S., Anglister, J., and Bax, A. (1993) *J. Magn. Reson., Ser. B 101*, 114−119.
39. Fesik, S., and Zuiderweg, E. R. P. (1988) *J. Magn. Reson. 78*, 588−593.
40. Kay, L. E., Keifer, P., and Saarinen, T. (1992) *J. Am. Chem. Soc. 114*, 10663−10665.
41. Bartels, C., Xia, T.-H., Billeter, M., Guntert, P., and Wuthrich, K. (1995) *J. Biomol. NMR 6*, 1−10.
42. Cornilescu, G., Delaglio, F., and Bax, A. (1999) *J. Biomol. NMR 13*, 289−302.
43. Wishart, D. S., and Sykes, B. D. (1994) *J. Biomol. NMR 4*, 171−180.
44. Wishart, D. S., Sykes, B. D., and Richards, F. M. (1992) *Biochemistry 31*, 1647−1651.
45. Lee, W., Revington, M. J., Arrowsmith, C., and Kay, L. E. (1994) *FEBS Lett. 350*, 87−90.
46. Laskowski, R. A., MacArthur, M. W., Moss, D. S., and Thornton, J. M. (1993) *J. Appl. Crystallogr. 26*, 283−291.
47. Brunger, A. T. (1996) *Xplor manual*, version 3.843, Yale University.
48. Kuszewski, J., Gronenborn, A. M., and Clore, G. M. (1996) *Protein Sci. 5*, 1067−1080.
49. Koradi, R., Billeter, M., and Wüthrich, K. (1996) *J. Mol. Graphics 14*, 51−55.
50. Kelley, L. A., Gardner, S. P., and Sutcliffe, M. J. (1997) *Protein Eng. 10*, 737−741.
51. Guo, W. (1999) Ph.D. Thesis, Cornell University.
52. Lamarche, N., Tapon, N., Stowers, L., Burbelo, P. D., Aspenström, P., Bridges, T., Chant, J., and Hall, A. (1996) *Cell 87*, 519−529.
53. Stevens, W. K., Vranken, W., Goudreau, N., Xiang, H., Xu, P., and Ni, F. (1999) *Biochemistry 38*, 5968−5975.
54. Tong, L., de Vos, A. M., Milburn, M. V., and Kim, S.-H. (1991) *J. Mol. Biol. 217*, 503−516.
55. Pai, E. F., Krengel, U., Petsko, G. A., Goody, R. S., Kabsch, W., and Wittinghofer, A. (1990) *EMBO J. 9*, 2351−2359.
56. Hart, M. J., Shinjo, K., Hall, A., Evans, T., and Cerione, R. A. (1991) *J. Biol. Chem. 266*, 20840−20848.
57. Seeburg, P. H., Colby, W. W., Capon, D. J., Goeddel, D. V., and Levinson, A. D. (1984) *Nature 312*, 71−75.
58. Krengel, U., Schlichtig, I., Schere, A., Schumann, R., Frech, M., John, J., Kabsch, M., Pai, E. F., and Wittinghofer, A. (1990) *Cell 62*, 539−548.
59. Franken, S. M., Scheidig, A. J., Krengel, U., Ronsland, H., Lautwein, A., Beyer, M., Scheffzek, K., Goody, R. S., Kalb, H. R., Pai, E. F., and Wittinghofer, A. (1993) *Biochemistry 32*, 8411−8420.
60. Leonard, D., Hart, M. J., Platko, J. V., Eva, A., Henzel, W., Evans, T., and Cerione, R. A. (1992) *J. Biol. Chem. 267*, 22860−22868.
61. Rittinger, K., Walker, P. A., Eccleston, J. F., Nurmahomed, K., Owen, D., Laue, E., Gamblin, S. J., and Smerdon, S. J. (1997) *Nature 388*, 693−607.
62. Nassar, N., Hoffman, G. R., Manor, D., Clardy, J. C., and Cerione, R. A. (1998) *Nat. Struct. Biol. 5*, 1047−1052.
63. Lian, L.-Y., Barsukov, I. L., Golovanov, A. P., Hawkins, D. I., Badii, R., Guo, W., Oswald, R. E., and Roberts, G. C. K. (1999) *J. Biol. Chem.* (submitted for publication).
64. Kelley, L. A., Gardner, S. P., and Sutcliffe, M. J. (1996) *Protein Eng. 9*, 1063−1065.
65. Kraulis, P. J. (1991) *J. Appl. Crystallogr. 24*, 946−950.
66. Merritt, E. A., and Murphy, M. E. P. (1994) *Acta Crystallogr., Sect. D 50*, 869−873.

BI992646D